Food Research International 121 (2019) 785–797

Contents lists available at ScienceDirect

Food Research International

journal homepage: www.elsevier.com/locate/foodres

Elucidating how two different types of bleaching earths widely used in vegetable oils industry remove carotenes from palm oil: Equilibrium, kinetics and thermodynamic parameters

Erislene S. Almeida[a], Ariane Cristina Boechie Carvalho[a], Isabela Oliveira de Souza Soares[a], Leonardo Fonseca Valadares[b], Andressa Regina Vasques Mendonça[a], Ivanildo José Silva Jr[c], Simone Monteiro[a,*]

[a] Institute of Chemistry, University of Brasília, Brasília, DF, Brazil
[b] Embrapa Agroenergia, Brasília, DF, Brazil
[c] Chemical Engineering Department, Federal University of Ceará, Ceará, CE, Brazil

ARTICLE INFO

Keywords:
Bleaching earth
Hybrid palm oil
Adsorption
Isotherm
β-carotene
Color inversion

ABSTRACT

This work compared the mechanisms of adsorption of carotenes from hybrid palm oil onto two kinds of bleaching earths widely used by industrial refiners (acid-activated and neutral). First, it was performed a deep characterization of adsorbent surfaces: acid activated adsorbent showed micropore volumes twice larger than the neutral. FTIR analysis of adsorbent after adsorption demonstrated that active site was Si–O–Si for both adsorbents. However, comparison of peak shapes suggested distinctive interactions between adsorbent/adsorbate for each adsorbent. Latterly, an extensive kinetic and equilibrium study was performed. Kinetic data were in accordance with pseudo-first and pseudo-second-order models. Adjusting to the intra-particle diffusion model evidenced more than one mechanism controlling the adsorption process. Equilibrium data demonstrated adsorption is only favorable at low carotene concentration at liquid phase for acid adsorbent (lower than 1 mg/mL). For neutral adsorbent, it was not clearly observed a favorable region with the studied conditions. The acid adsorbent could adsorb more carotenes per adsorbent weight than neutral. Finally, neutral adsorbent showed higher heterogeneity of interaction between adsorbate and adsorbent than the acid, especially at low adsorbent coverages.

1. Introduction

Palm oil is currently the most consumed edible oil in the world (USDA, 2018). Moreover, it is the crop with the highest productivity per hectare, being up to 10 times more productive than soybean oil, for instance, therefore, palm oil highly competitive in the market. Population growth in emerging markets, expansion by the food processing industry, replacement of hydrogenated oils by a *trans*-fat-free and utilization for biofuel production have all contributed to more than doubling its consumption over the past 15 years. Also, the demand for palm oil consumption tends to keep growing (Norizzah, Nur Azimah, & Zaliha, 2018; Pirker, Mosnier, Kraxner, Havlík, & Obersteiner, 2016).

Prior to human consumption, crude palm oil undergoes a refining process that aims at removing compounds such as phospholipids, free fatty acids, oxidation products, pigments, and other undesirable components. Refining process is crucial to ensure the final product quality (odor, flavor, color), as well as its function (fatty acids composition, vitamins and antioxidants) and its cost (neutral oil loss). Besides its provitamin A activity, it is imperative to remove carotenes from palm oil once they are responsible for the dark orange color, that would derail its use in a wide range of food and pharmaceutical products such as ice creams, breads, margarines and cosmetics (Ribeiro, Almeida, Neto, Abdelnur, & Monteiro, 2018). Palm oil is preferably refined by the physical method due to its high free fatty acids content, as the use of caustic substances to remove them would result in large amounts of soap and neutral oil loss (Sampaio et al., 2017; Silva et al., 2013). In this type of refining, free fatty acids are removed by volatilization at high temperatures and very low pressures. However, it is still necessary to pre-treat oil by degumming and bleaching, in order to remove impurities that cause a change in color and other quality losses when heating the oil (Gibon, De Greyt, & Kellens, 2007). As a matter of fact, color is a major problem for the industry, once it is desired that palm oil

* Corresponding author at: Instituto de Química, Universidade de Brasília, Campus Universitário Darcy Ribeiro, 70910-000 Brasília, DF, – Brasil.
E-mail address: simonems@unb.br (S. Monteiro).

https://doi.org/10.1016/j.foodres.2018.12.061
Received 21 July 2018; Received in revised form 28 December 2018; Accepted 30 December 2018
Available online 02 January 2019
0963-9969/

be light yellow in color, guaranteeing its versatility and the use in diverse products (Ribeiro et al., 2018; Silva et al., 2014).

Palm oil color is fundamentally due to α- and β-carotenes (Ng & Choo, 2016; Ribeiro et al., 2018), which are mostly removed by an adsorptive process called bleaching. This process also aims to remove other pigments (e.g. chlorophylls), metals (iron and copper), soaps and oxidation products (Sampaio et al., 2017). Adsorbents such as activated carbon, silica and acid activated clays are commonly used in the industry (Pohndorf, Cadaval, & Pinto, 2016).

The full reduction of carotenes by bleaching is not necessary, as they can be thermally decomposed during the subsequent deacidification (known as heat bleaching) (Gibon et al., 2007), by thermal decomposition and/or oxidation reactions (Gurak, Mercadante, González-Miret, Heredia, & Meléndez-Martínez, 2014). β-carotene thermal degradation in fatty systems follows first-order kinetics (Calligaris, Valoppi, Barba, Anese, & Nicoli, 2018). At deacidification temperatures (above 200 °C), total carotenes degradation follows a 1.3 order kinetics, probably due to synergetic antioxidant effects with tocopherols (Sampaio et al., 2013). Consequently, only 20% of carotenoid is removed during bleaching by industrials, the remaining is destroyed by heat bleaching (Gibon et al., 2007; Maclellan, 1983).

Nevertheless, there is no correlation between β-carotene content after bleaching and the final color of palm oil. Studies have suggested that this color is due to high molecular weight compounds derived from oxidation reactions, especially in the case of carotenoids. In addition, very aggressive bleaching conditions, such as excessive temperatures or time process or both, also leads to darker final colors (Silva et al., 2014). The authors carried out several fully physical refining procedures (bleaching and deacidification) using different amounts of both Pure Flo B 80 (neutral) and Tonsil OPT 210 FF (acid). Both adsorbents were able to reduce palm oil color, however, oil bleached with neutral adsorbent presented lower total carotenoids content when compared with acid adsorbent. The same oil presented a darker color after deacidification, showing a lower color reduction due to heat bleaching. Presented experimental data was not able to explain this behavior. Furthermore, there is some evidence that the adsorbent used during palm oil bleaching catalyzes the β-carotene isomerization, interfering, therefore, in the color of fully refined palm oil (Silva et al., 2014). External agents, such as oxidants, light and heat, induces E/Z isomerization of carotenes (Gurak et al., 2014). More recently, Ribeiro et al. (2018) evaluated the carotenoids isomers remaining in oil bleached with different types of adsorbents widely used in the vegetable oil industry: the concentration of α-carotene after adsorption process was considerably different, reflecting selective adsorption between carotenoids isomers. The authors indicate that further studies are necessary to explain this different behavior.

Most commercial oil palm plantations are *E. guineensis*, an African cultivar which is high productivity per hectare. However, it is very susceptible to diseases, such as fatal yellowing, that is important especially in South America. *E. oleifera*, cultivar originally from Central and South America is more resistant to illness. However, this is underexploited commercially due to low productivity (España et al., 2018). Hybridization between the African and American oil palm generated a cultivar both highly productive and resistant (Mozzon, Pacetti, Lucci, Balzano, & Frega, 2013). However, there is a lack of scientific studies about the processing of palm oil from the hybrid cultivar.

In this context, the objective of this work was to evaluate the differences on carotenes adsorption from Hybrid Crude Palm Oil (CPO) onto two commercial bleaching earths: one acid activated (Tonsil OPT 210 FF) and one neutral (Pure Flo B 80). Therefore, bleaching experiments were performed under industrial similar conditions, i.e. high temperature, low pressure and without solvent. Kinetic and equilibrium adsorption parameters were measured in the carotenes adsorption from palm oil by using commercial adsorbents. Adsorbents characterization prior to and after adsorption process were performed to elucidate differences on mechanisms.

2. Material and methods

2.1. Adsorbent

The adsorption experiments were performed using two types of commercial bleaching earths widely used in the vegetable oil industry: the acid activated adsorbent (ABE) Tonsil OPT 210 FF, manufactured by acid activation of calcium bentonite, which was kindly provided by Clariant (Germany); the neutral adsorbent (NBE) Pure Flo B 80, composed by bentonite, that was kindly provided by Oil Dri (USA).

2.2. Adsorbent Characterization

Brunauer–Emmett–Teller (BET) surface area measurements were performed using a Quantachrome Autosorb iQ3 at liquid nitrogen temperatures. Prior to experiments, samples were degassed under vacuum and at a heating rate of 1 °C/min up to 120 °C, then they were sustained at these conditions for 6 h.

The material surface morphology, before and after adsorption experiments, were evaluated by scanning electronic microscopy (SEM). Adsorbents after adsorption process using 3% (weight of adsorbent/weight of oil) and at 90, 105 and 120 °C were firstly dried in an oven (TE-395, TECNAL, Brazil) at 50 °C during 48 h. Both adsorbents before and after adsorption were covered by a 10 nm gold layer in the sputter coating unit (SCO050, Balzers, Austria) during 2.5 min at 40 μA. Then, scanning electron microscopy characterization was conducted at 30 kV and 120.4 μA (JSM-7001F, JEOL, USA).

Moreover, FTIR spectra of adsorbents before and after adsorption process were recorded in an infrared spectrophotometer (Affinity-1, Shimadzu, Japan) using solid samples dispersed in KBr pellets (each one constituted by about 1 mg of sample and 99 mg KBr) with a spectrum range 400–4000 cm^{-1} to observe different functional groups.

2.3. Oil characterization

Crude palm oil from a hybrid cultivar (*Elaeis guineensis* × *Elaeis oleifera*) was kindly supplied by Denpasa (Santa Bárbara do Pará, PA, Brazil). The oil sample was characterized regarding the standard quality parameters. Free fatty acid (FFA) content was determined by titration according to the official method Ca 5–40 (AOCS, 1998): about 2.0 g of oil samples were diluted in 40 mL 50:50 (*v*/v) ethanol/ethyl ether solution and titrated with sodium hydroxide solution (0.1 mol/L). FFA results were expressed as percentage of palmitic acid (Eq. 1).

$$FFA(\%) = \frac{V_{NaOH} \cdot N_{NaOH} \cdot 256.4}{m_{sample} \cdot 10} \quad (1)$$

where V_{NaOH} is the volume of sodium hydroxide solution spent for titration; N_{NaOH} is the normality of hydroxide solution (0.1 mol/L); and m_{sample}(g) is the exact mass of sample that was titrated. Each mol of fatty acid was considered to present the molar mass of palmitic acids (256.4 g/mol). Total carotene content, expressed as β-carotene, was determined by UV–vis spectrometry (Spectrophotometer SpectraMax M3, Molecular Devices, USA) measuring the absorbance at 445 nm (Silva et al., 2014). Hexane (HPLC/UV, > 95%, Macron, USA) was used as the solvent. β-carotene solutions (Sigma Aldrich) were used as the standard to construct the calibration curve, which consisted of 10 experimental points ranging from 0.2 to 2.0 mg/L. Quantification was performed by linear fitting ($R^2 > 0.99$). For sample preparation, about 0.04 g of oil was diluted in 10 mL of hexane.

2.4. Adsorption experiments

Batch adsorption experiments were carried out according to the methodology adapted from Silva et al. (2013), reproducing industrial bleaching of palm oil. In each test, 50 g of crude palm oil was placed into 100 mL flasks and heated to 90 °C (Rotavapor, Gehaka, RD 180,

Brazil). Then, the following steps were performed: addition of 0.09% m/m of citric acid (to chelate metals), as a 30% *w*/w aqueous solution; high shear mixing at 15,000 rpm to allow contact between aqueous and oil phases (mixer, Turratec, Tecnal, Brazil); maintaining the mixture at the selected temperature under atmospheric pressure during 15 min; addition of the selected adsorbent (bleaching earth); vacuum application to avoid oxidation reactions (< 50 mbar of absolute pressure) during the selected time and temperature. The adsorption process was interrupted by removing the bleaching earth, what was done by filtration over Buchner funnel and paper filter (pore size 11 μm, Whatman). Kinetics of adsorption was determined using 3%$_{(w/w)}$ at agitation time ranging from 0 to 120 min and temperature at 90, 105 and to120 °C. The adsorption isotherms were obtained in 30 min experiments with different concentrations of bleaching earth (ranging from 0.1 and 9.0 wt%) using the same kinetic experiments conditions.

Furthermore, blank runs (without adding adsorbent) were made to evaluate the thermal degradation in all tested conditions mentioned above. The experiment was performed according to the procedure previously described at temperature ranging from 90, 105 to 120 °C. The initial and final concentrations of total carotenes were measured by UV–vis spectrometry (see Section 3.1).

The adsorbate concentrations in solid phase q_t (mg/kg) at time t, were obtained by mass balance, according to Eq. 2:

$$q_t = \frac{W_{oil}(C_0 - C_t)}{W_{BE}} \quad (2)$$

where W_{oil} is the weight of crude palm oil treated in kg, W_{BE} is the weight of bleaching earth in kg, C_0 is the initial concentration of carotenes in (mg/kg), C_t is the liquid phase concentration of adsorbate at time t (min), respectively. After equilibrium time, adsorbate concentration at the solid phase and the liquid phase becomes q_e and C_e, respectively.

2.5. Modeling

Adsorption models were fitted to experimental data using nonlinear regression analysis performed using *MatLab Curve Fitting Tool*™ and Levenberg-Marquardt interactive method. The parameters and coefficients of determination (R^2) were obtained at 95% confidence interval. For the BET isotherm adjustments, the equilibrium constant of the first layer was fixed using the value of this constant found by the Langmuir adjustment.

2.6. Adsorption kinetics

2.6.1. Pseudo-first-order rate equation

The pseudo-first-order equation can be expressed in a non-linear (Eq. 3) (Yousef, El-Eswed, & Al-Muhtaseb, 2011).

$$q_t = q_e(1 - exp(-k_1 t)) \quad (3)$$

where q_t and q_e are adsorption capacity at time t and at equilibrium e, respectively, i.e., the amount of adsorbate per unit of adsorbent; k_1 is the pseudo-first-order constant t^{-1}. Please note that this model is based on adsorption capacity instead of solution concentration. Typically, this model is suitable to describe the first 20–30 min of the adsorption process (Silva et al., 2013).

2.6.2. Pseudo-second-order rate equation

The pseudo-second-order equation can be expressed in a non-linear equation (Eq. 4) (Yousef et al., 2011).

$$q_t = \frac{q_e^2 k_2 t}{1 + q_e^2 k_2 t} \quad (4)$$

where k_2 is the pseudo-second-order constant t^{-1}. The pseudo-second-order equation is based on the adsorption capacity of the solid phase and it is in agreement with chemisorption being the rate controlling step (Ho & McKay, 1998). In the same way, Ho's second order-equation has been a so-called pseudo-second-order rate equation to distinguish from the one based on the solution concentration.

Table 1
Textural properties calculated from adsorption of nitrogen at 393 K.

Adsorbnt	Specific Surface area	Pore Volume	Micropore Volume
	(m^2/g)	(cm^3/g)	(cm^3/g)
ABE Tonsil OPT 210FF	269	0.362	0.104
NBE Pure Flo B-80	174	0.273	0.067

2.6.3. Intra-particle diffusion

The Weber-Morris intra-particle diffusion model is expressed as (Eq. 5);

$$q_t = k_{id} t^{0.5} + C_i \quad (5)$$

where k_{id} (mg/kg min$^{0.5}$) is the intra-particle diffusion rate constant and C_i (mg/kg) is associated to the boundary layer thickness. If intra-particle diffusion is the limiting step of the adsorption process, the plot q_t against $t^{0.5}$ is a straight line. Moreover, if this plot goes through the origin, intra-particle diffusion is the only rate-limiting step (Silva et al., 2013); if the plot presents two or more intercepting straight lines, adsorption involves independent steps (Alkan, Demirbaş, & Doğan, 2007).

2.7. Equilibrium studies

The isotherm parameters correlate the kinetics and thermodynamics of the adsorption process, providing a quantitative and qualitative estimation of the efficiency of the adsorbent (Ghosal & Gupta, 2017). In this work, three adsorption isotherms were used to evaluate adsorption of carotenes onto bleaching earth: Langmuir, Freundlich and BET.

2.7.1. Langmuir

The Langmuir model was the first model presenting a coherent theory of adsorption. It assumes a monolayer surface coverage, an independent and homogeneous adsorbent surface, mostly applied to chemisorption (Ghosal & Gupta, 2017; Silva et al., 2013). It is generally expressed in a non-linear model (Eq. 6):

$$q_e = \frac{q_{max} K_S C_e}{1 + K_S C_e} \quad (6)$$

where q_e (mg/kg) is the amount of adsorbate per unit mass of adsorbent, C_e (mg/kg) is the equilibrium concentration of adsorbate in solution, q_{max} (mg/kg) and K_S (mg/kg)$^{-1}$ are Langmuir constants related to the adsorption capacity at equilibrium and rate of adsorption for the monolayer, respectively.

2.7.2. Freundlich

The Freundlich model is an empirical one, assuming a heterogeneous surface energy, i.e., stronger binding sites are occupied first and the binding strength decreases with an increasing degree of site occupation (Yousef et al., 2011) and it is not restrictive to monolayer coverage. It is generally described in its non-linear form (Eq. 7):

$$q_e = K_F C_e^n \quad (7)$$

where K_F [(mg/kg)(mg/kg)$^{-n}$]is defined as the adsorption capacity of the adsorbent. The n values range from zero to one, reflecting the adsorption intensity or surface heterogeneity.

2.7.3. BET model

The theoretical model, firstly proposed by Brunauer, Emmett and

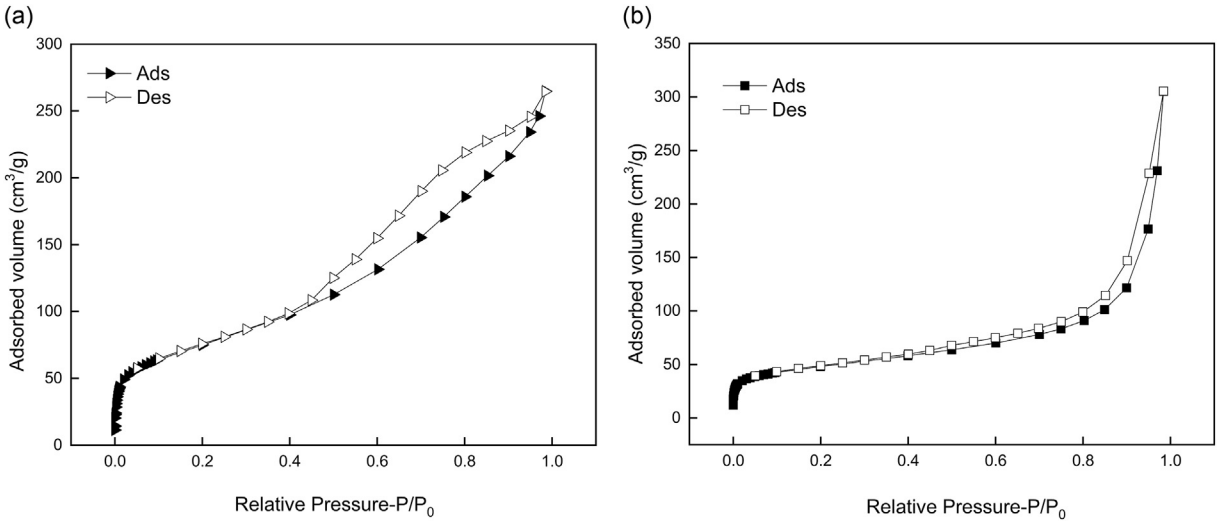

Fig. 1. Nitrogen adsorption isotherms at 393 K of: (a) acid activated adsorbent (ABE, Tonsil OPT 210 FF) and (b) neutral adsorbent (NBE, Pure Flo B-80).

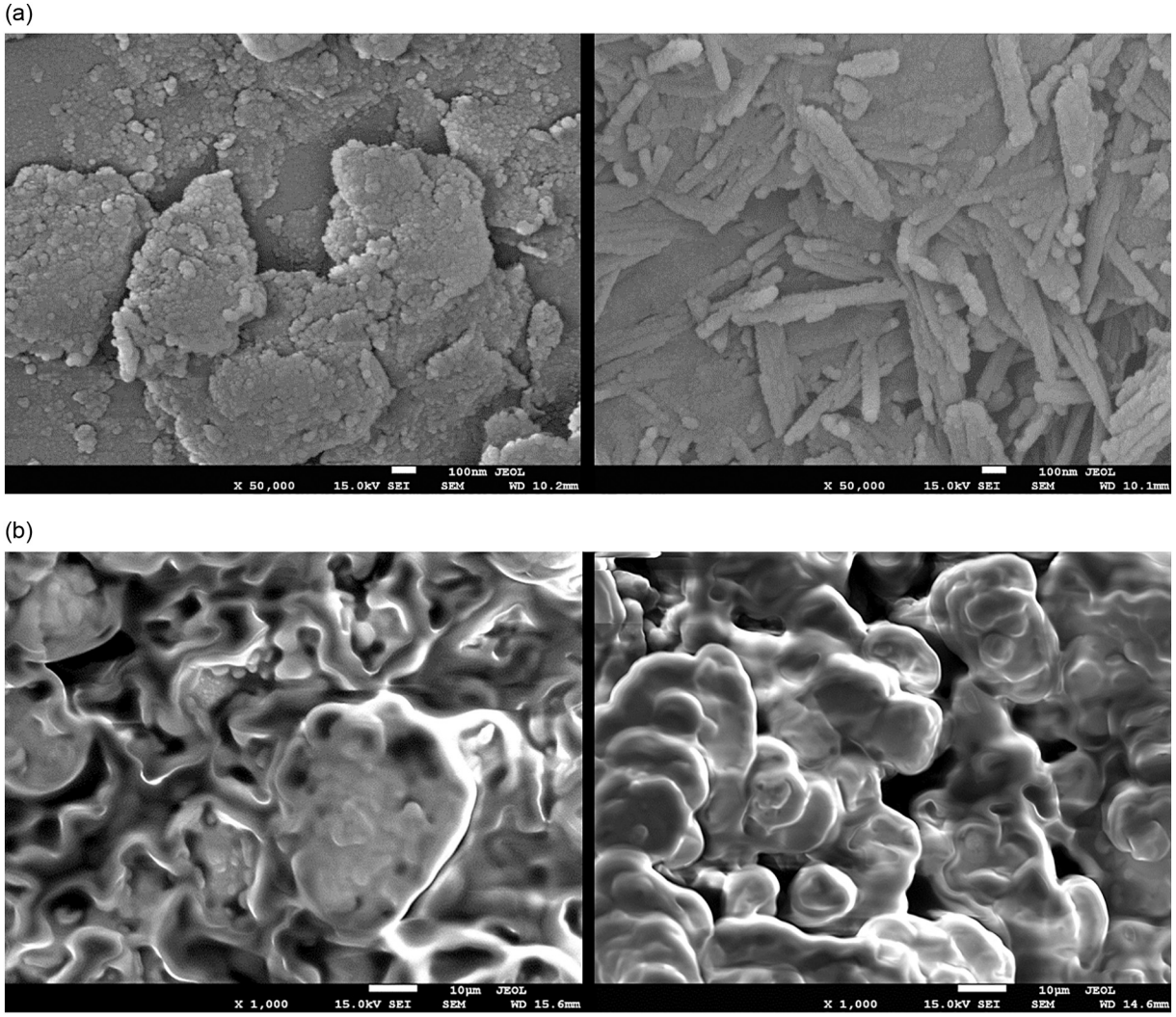

Fig. 2. SEM images of adsorbents prior (a) and after adsorption process (b): *left* acid activated adsorbent (ABE, Tonsil OPT 210 FF) and *right* neutral adsorbent (NBE, Pure Flo B-80).

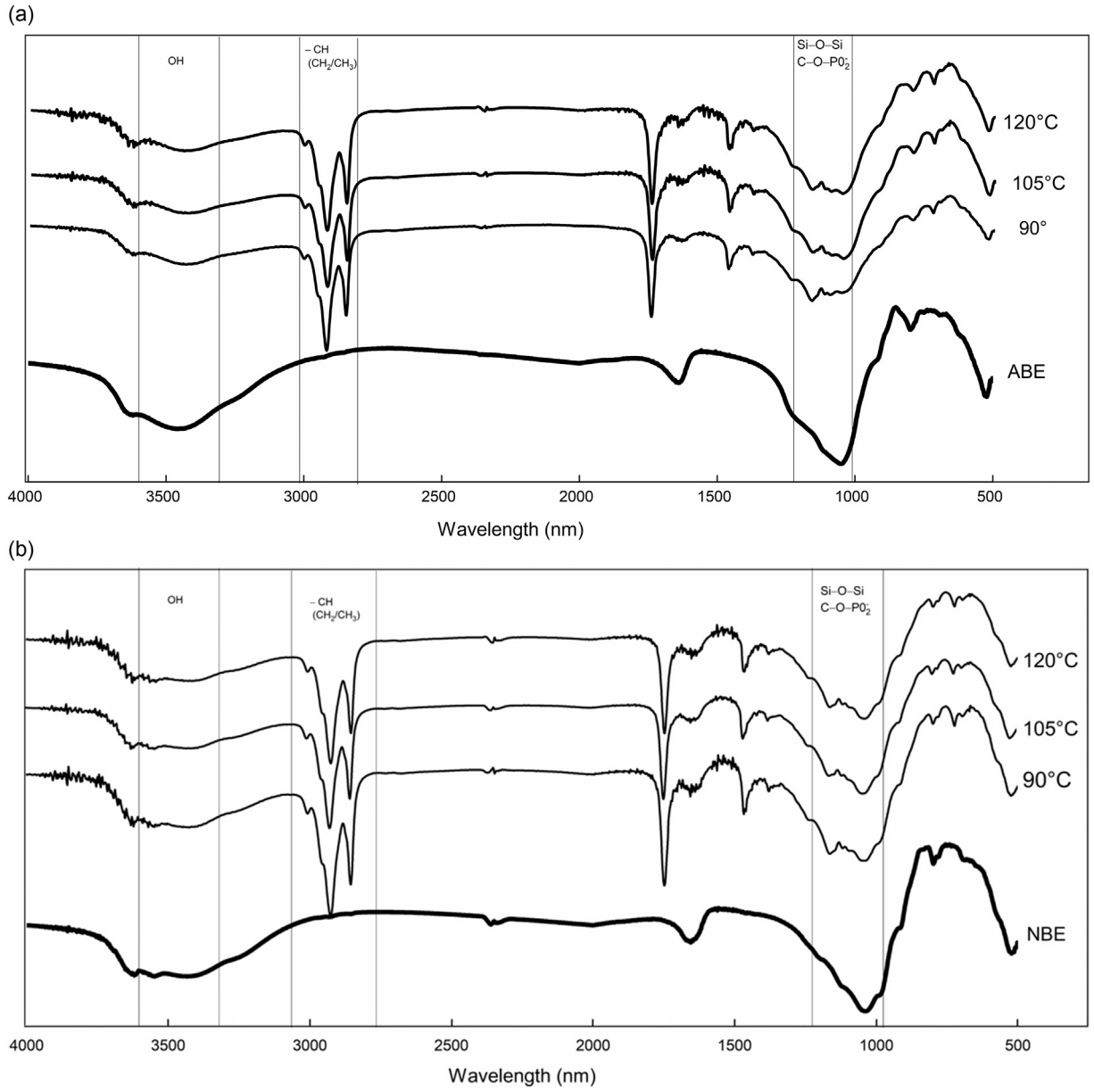

Fig. 3. FTIR spectra of adsorbents prior and after adsorption using 3.0 wt%: (a) acid activated adsorbent (ABE, Tonsil OPT 210 FF) and (b) neutral adsorbent (NBE, Pure Flo B-80).

Teller (BET), considers that gas phase adsorption occurs by multiple layers. Due to its great success to describe this adsorption process, lately, it has been adapted to describe liquid phase adsorption by a three-parameter model (Ebadi, Soltan Mohammadzadeh, & Khudiev, 2009).

$$q = q_{max}\frac{K_s C_e}{(1 - K_l C_e)(1 - K_l C_e + K_s C_e)} \quad (8)$$

where K_s (g/mg) and K_l (g/mg) are the equilibrium adsorption constants for the first layer and upper layers, respectively.

2.8. Thermodynamics parameters

The Standard Gibbs Free Energy can provide the degree of exoergicity and the higher its absolute value reflects more energetically favorable adsorption. Whereas, enthalpy is important to determine whether the adsorption process in chemical or physical, as it is shown in Eq. 9:

$$\Delta G^0_{ads} = -RTln(K_0) \quad (9)$$

where $\Delta G_{ads}{}^0$ (J/mol) is the standard Gibbs Free Energy, R is the universal gas constant (8.3145 J·mol^{-1}·K^{-1}), T (K) is the temperature, and K_0 is the *equilibrium* constant (or the solute coefficient of distribution between the solid and liquid phases at *equilibrium*) which changes with temperature. The coefficient K_0 was obtained by applying limit to the curve $\ln(q_e/c_e)$ vs q_e for each adsorbent and temperature (Eq. 10).

$$K_0 = \lim_{q_e \to 0} \frac{q_e}{C_e} \quad (10)$$

Standard Gibbs Free Energy might be expressed in terms of standard enthalpy

($\Delta H_{ads}{}^0$) and standard entropy ($\Delta S_{ads}{}^0$) according to van't Hoff equation (Eq. 11) (Garvín, Ibarz, & Ibarz, 2017).

$$\ln(K_0) = -\frac{\Delta G^0_{ads}}{RT} = \frac{\Delta S^0_{ads}}{R} - \frac{\Delta H^0_{ads}}{RT} \quad (11)$$

The isosteric heat of adsorption ($\Delta H_{st,\,a}{}^0$) is the change of adsorption

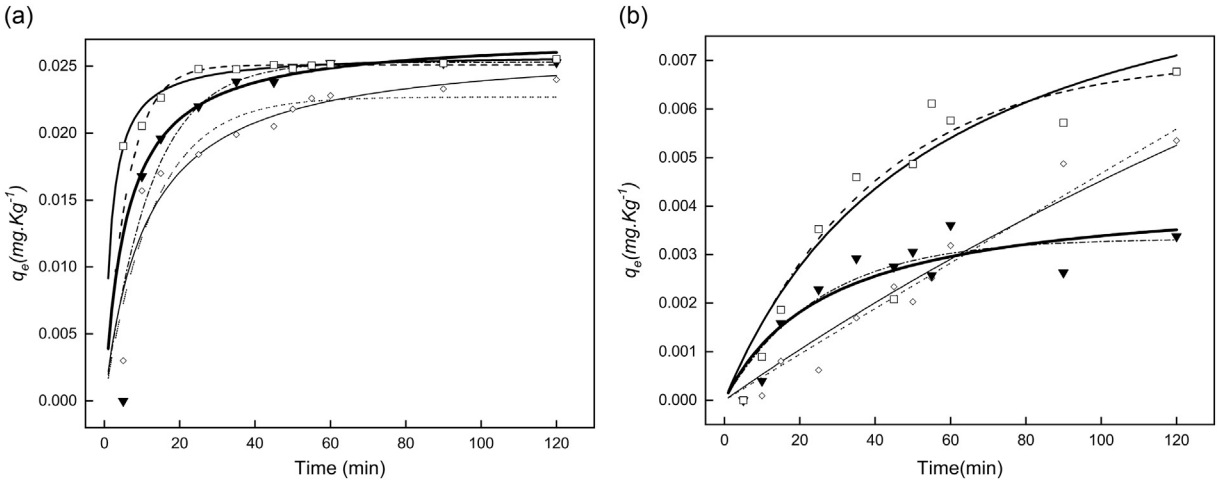

Fig. 4. Adsorption kinetics of Carotenes onto ABE (a) and NBE (b) at 90, 105 and 120 °C and using 3.0 wt% of bleaching earth.

enthalpy at a constant number of adsorbed molecules at two or more temperatures (Builes, Sandler, & Xiong, 2013). Equilibrium concentrations at a constant number of adsorbed compounds were calculated by BET isotherm. The isosteric heat of adsorption was obtained from plot slope of ln (C_e) versus ($1/T$) for different amounts of adsorbed carotenes (Eqs. 12 and 1):

$$\frac{d(ln\ C_e)}{dt} = -\frac{\Delta H_{st,a}}{RT^2} \tag{12}$$

$$\Delta H_{st,a} = \mathrm{R}\left(\frac{\mathrm{d}(ln\, C_e)}{\mathrm{d}(1/T)}\right)_{q_e} \tag{13}$$

where $\Delta H_{st,\ a}$ (J/mol) is the isosteric heat of adsorption.

3. Results and discussion

3.1. Adsorbent characterization

3.1.1. Textural properties

Table 1 summarizes the textural characterization of the adsorbents obtained from the isotherms presented in Fig. 1, both samples presenting high surface areas. It can be seen that ABE presented higher surface area (269 m^2/g) than NBE (174 m^2/g), which is a result of the activation process. Furthermore, ABE presented higher volumes of pore and micropore. The larger surface area along higher volumes of pore and micropore of ABE allow the oil to enter pore cavities more easily, and consequently, improves the access of adsorbate to the adsorption sites inside pore cavities. However, it may result in a larger amount of oil impregnated at the end of the adsorptive process (Gibon et al., 2007). Characteristic hysteresis loop presented by isotherms characterized show that they are Type VI, typical of mesoporous materials (20 to 500 Å) (Alhamami, Doan, & Cheng, 2014). Large hysteresis loop of ABE is attributed to disordered mesoporous materials such as porous glasses and silica gels (Morishige, Tateishi, & Fukuma, 2003).

3.1.2. Scanning electronic microscopy

Fig. 2a shows secondary electronic images of the samples. Differences of morphology could be observed between the studied materials. In both adsorbents, it can be noted that the particles that constitute them did not present regular sizes and shapes. ABE is formed by overlapping plates, constituted by small granules. On the other hand, NBE consists of agglomerates of small filaments. The morphological differences between the particles constituting the materials may account for changes in the adsorption efficiency of carotenes, for example, the adsorbent that underwent the acid treatment to present a larger surface area of contact. Fig. 2b presents images for each adsorbent after the adsorption process. It could be observed an oil layer above the adsorbent surface and its morphology became rounded.

3.1.3. Infrared spectroscopy

The infrared spectra were obtained for the crude oils and for the adsorbents before and after adsorption process with 3.0% at 90, 105 and 120 °C in a wavenumber range of 400–4000 cm^{-1} (Fig. 3). Both adsorbents presented a broad band in the region 3500–3400 cm^{-1} and 1654 cm^{-1} attributed to octahedral layer and hydroxyl stretching, respectively. The peaks at 3619 and 916 cm^{-1} are characteristics of dioctahedral smectites. The bands at 1050 and 1040 cm^{-1}, for acid activated and neutral adsorbents respectively, are attributed to Si–O–Si stretching; and 798 cm^{-1} attributed to Fe^{3+}–OH–Mg (Alabarse, Conceição, Balzaretti, Schenato, & Xavier, 2011).

In addition, adsorbent spectra before and after the adsorption process were quite similar. The most important difference was in the region between 1115 and 900 cm^{-1}, for adsorbent after the process at 90 °C. The presence of adhered oil in the adsorbent surface can be noted by the presence of following bands: at 2924 cm^{-1} and 2852 cm^{-1} attributed to C–H (CH_2) asymmetric and symmetric stretching; at 3005 cm^{-1} attributed to C–H (CH_3) stretching; at 1745 cm^{-1} attributed to C═O ester; at 1745 cm^{-1} corresponding to C═C weak stretching; at 1456 cm^{-1} and 1361 cm^{-1} of scissoring (bending) of C–H (CH_2) and C–H (CH_3), respectively; at 720 cm^{-1} attributed to HC═CH out-of-plane stretching (Lampman, Kriz, Vyvyan, & Pavia, 2010). All previously mentioned functional groups are found in fatty acids. At 1162 cm^{-1}, there was a reduction of a peak attributed to C–O–PO_2^- stretching, functional group commonly found in phospholipids, indicating their adsorption. After the adsorption process, the intensity of the band in the region of 3700 to 3400 cm^{-1} decreased, what evidences the water release (adsorbent natural humidity) due to heating (Norizzah et al., 2018).

Moreover, infrared spectroscopy demonstrated some difference in interactions between adsorbents and palm oil: the band 1300–1000 cm^{-1} (Si–O–Si) presented intensity and shape alteration after adsorption for ABE, whilst this band presented only intensity alteration for NBE. The peak of approximately 1050 cm^{-1} almost disappeared at 90 °C (Fig. 3), which shows the interaction between hybrid palm oil and adsorbents.

3.2. Oil Characterization

The crude oil was characterized regarding free fatty acids (FFA), DOBI value and total carotenes. Free fatty acids were 1.9%, expressed as palmitic acid, the result that corroborates what was previously reported for the oil obtained from hybrid cultivar (Mozzon et al., 2013).

Table 2
Fitting kinetics and mechanism parameters of adsorption of carotene onto acid activated and neutral bleaching earths according to pseudo-first-order, pseudo-second-order and intra-particle diffusion at 90, 105 and 120 °C.

		ABE					NBE				
Model	Parameters	90 °C	t-value	105 °C	t-value	120 °C	t-value	90 °C	t-value	105 °C	t-value	120 °C	t-value
Langmuir	K_s	22.91 ± 2.7	52.725	17.47 ± 2.24	38.5	12.38 ± 3.093	4.00						
	q_m	29.22 ± 0.5	8.365	40.67 ± 1.06	7.81	55.99 ± 3.83	14.63						
	R^2_{adj}	0.969		0.970		0.913							
	F-test	3063		1551		276							
	P-value (95%)	< 0.0001		< 0.0001		< 0.0001							
Freundlich	K_f	28.58 ± 0.7	43.43	39.92 ± 1.94	20.59	58.50 ± 4.010	14.58						
	n	0.145 ± 0.02	7.63	0.204 ± 0.04	5.262	0.311 ± 0.05	6.098						
	R^2_{adj}	0.941		0.870		0.903							
	F-test	1583		357		247							
	P-value (95%)	< 0.0001		< 0.0001		< 0.0001							
BET	K_s	22.91		17.47		12.38		2.74		8.56		7.88	
	K_l	0.44 ± 0.02	23.76	0.43 ± 0.03	14.60	0.58 ± 0.01	85.83	0.487 ± 0.015	33.26	0.659 ± 0.002	264.73	0.363 ± 0.051	7.137
	q_m	18.72 ± 1.7	11.26	27.24 ± 3.52	7.73	27.51 ± 1.84	14.93	4.43 ± 0.58	7.64	10.04 ± 1.47	6.83	13.06 ± 2.48	5.25
	R^2_{adj}	0.906		0.827		0.97		0.859		0.960		0.577	
	F-test	490		206		620		410		213		188	
	P-value (95%)	< 0.0001		< 0.0001		< 0.0001		< 0.0001		< 0.0001		< 0.0001	

*q_e (mg·kg^{-1}); k_1 (min^{-1}); k_2 (kg/mg.min^{-1}); K_{id}: (mg/Kg^{-1} .min$^{0.5}$).

Total carotene content was 1757 mg·kg^{-1}.

3.3. Adsorption experiments

3.3.1. Kinetics

Firstly, we performed blank runs to evaluate thermal degradation during the adsorption process, as carotenes are thermolabile. The plot percentage thermal degraded is presented in the Supplementary Material (Fig. S1). For all temperatures, the percentage degraded during the first 90 min was lower than 8.5%. Besides that, for the temperatures of 90 and 105 °C, it can be noted some points in that degradation presented negative values, evidencing that concentration variation is in the range of analysis intrinsic error. In this way, we considered in this work that any decrease in carotenes concentration was due to adsorption. As a matter of fact, the high concentration of tocopherols and tocotrienols in palm oil protects carotenes from thermal degradation (Sampaio et al., 2013).

The concentration plot of adsorbed carotene versus contact time are shown in Fig. 4 and the pseudo-first-order and pseudo-second-order parameters were determined by non-linear fitting (Table 2). Regarding adsorption onto ABE, it was noted higher determination coefficients and lower relative errors for the pseudo-second-order ($R^2 > 0.95$ and RMSE < 1.84) than for pseudo-first model ($R^2 > 0.88$ and RMSE < 2.13). This result is in agreement with those reported by Silva et al. (2013) for carotenes adsorption from native palm oil (*E. guineensis*) onto the same adsorbent (Tonsil OPT 210 FF). When experimental data are compared with predicted results, it can be seen that both models are good to describe the studied adsorption region, and the q_e values predicted present a good agreement with experimental data. Amount adsorbed at different temperatures presented similar results, being the differences lower than standard deviation. Adsorption process reached *equilibrium* after 30, 25 and 20 min for the process at 90, 105 and 120 °C, respectively. From this, we can conclude that different process temperature only affects the process speed, not affecting the maximum adsorption capacity. That is why we have set 30 min for the equilibrium experiments.

Regarding adsorption onto NBE, it was also observed higher determination coefficients and lower relative errors for the pseudo-first-order ($R^2 > 0.94$ and RMSE < 0.60) than for pseudo-second model ($R^2 > 0.93$ and RMSE < 0.66) for experimental data at 90 and 120 °C. Besides, the predicted parameters were not in good agreement with experimental data at 105 °C, as for this data set R^2 were 0.85 and 0.81 for pseudo-first and pseudo-second-order-models, respectively.

3.3.2. Intra-particle diffusion

The curve-fitting plot of the intra-particle model (q_e vs $t^{0.5}$) is shown in Fig. 5 and their parameters were determined by linear regression (Table 2). The plot for adsorption onto ABE presented two (at 120 °C) or three straight lines (90 °C and 105 °C) suggesting intra-particle diffusion is not the sole controlling step (Alkan et al., 2007). Almost all correlation coefficients were high ($R^2 > 0.93$), except for the straight lines corresponding to final steps (*equilibrium*) of the adsorption process. Adsorption process onto the acid activated bleaching earth present three independent steps: (1) diffusion across the liquid film surrounding the adsorbent particle; (2) diffusion in the liquid contained in the pores and/or along pore walls, so-called intra-particle diffusion; (3) final equilibrium step (Gonsalvesh, Marinov, Gryglewicz, Carleer, & Yperman, 2016; Liu, Ying, Sanguansri, Cai, & Le, 2018). The oil lower viscosity at 120 °C (Ceriani, Gonçalves, & Coutinho, 2011) resulted in a two-step process, due to the lower resistance of oil flowing inside the adsorbent pore.

Furthermore, adsorption onto NBE presented only one (at 90 °C) or two (at 105 and 120 °C) straight lines. Correlation coefficients were high ($R^2 > 0.93$), except for the *equilibrium* step. At 90 °C, the adsorption process occurred in a single step. This behavior may be explained by the high oil viscosity at this temperature allied to small pore

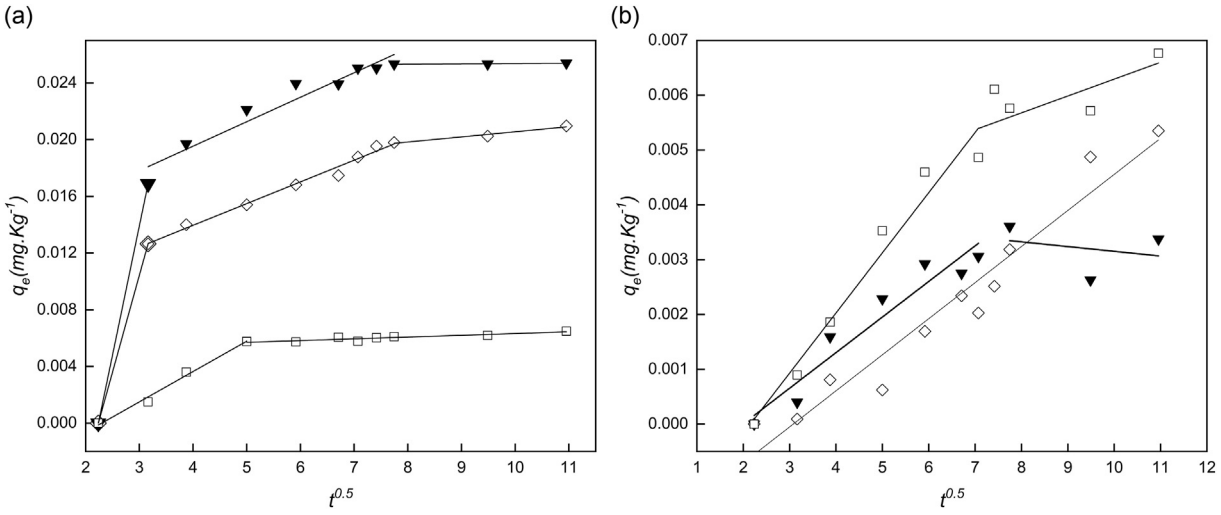

Fig. 5. – Intra-particle diffusion plots for the adsorption of carotenes onto ABE (a) and NBE (b) at 90 (◊), 105 (▼) and 120 °C (□)and using 3.0 wt% of bleaching earth.

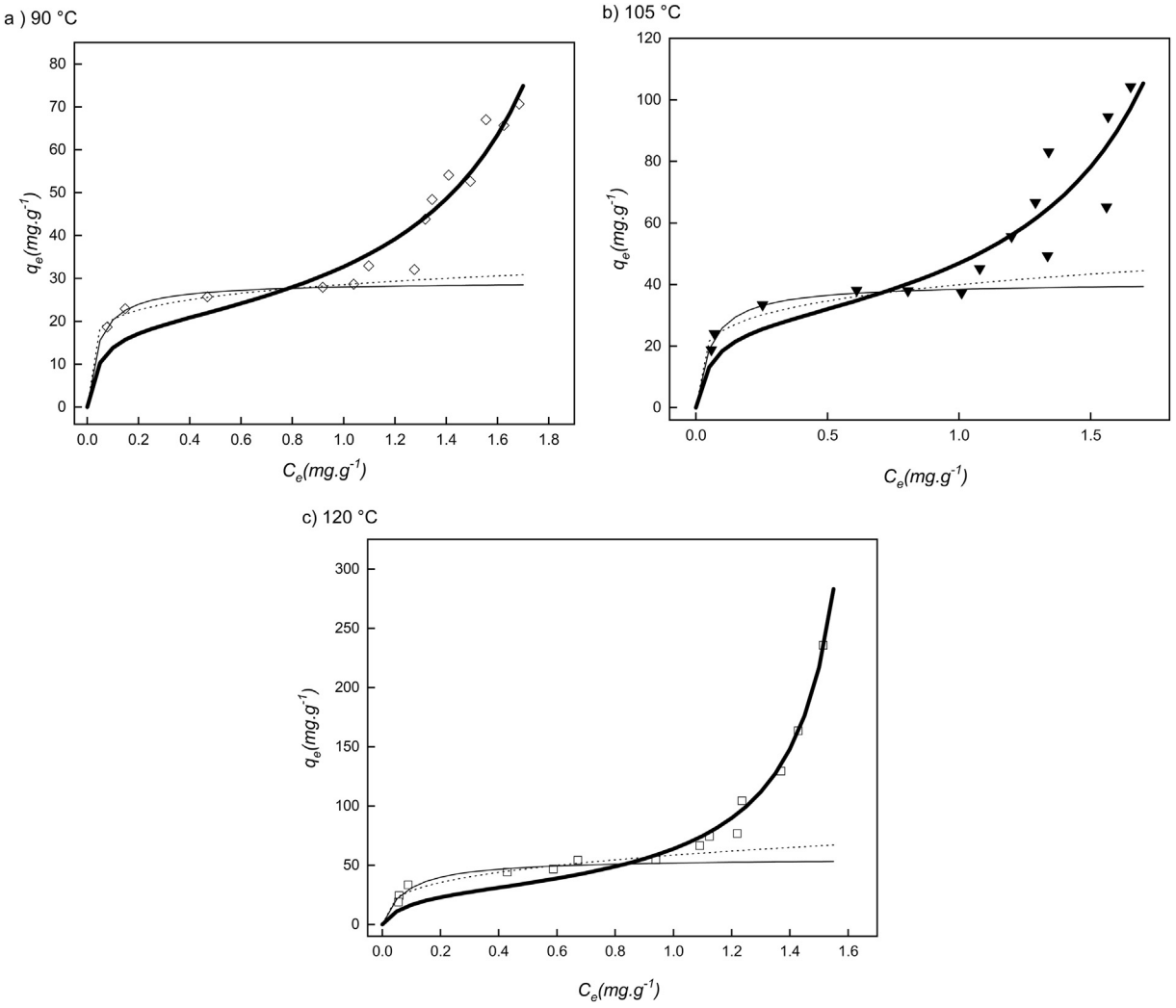

Fig. 6. Adsorption isotherm plots for carotenes onto ABE at (A) 90 °C, (B) 105 °C and (C) 120 °C. Representation: Experimental data – symbols, modelled – lines: Langmuir (solid), Freundlich (dashed), BET (bold).

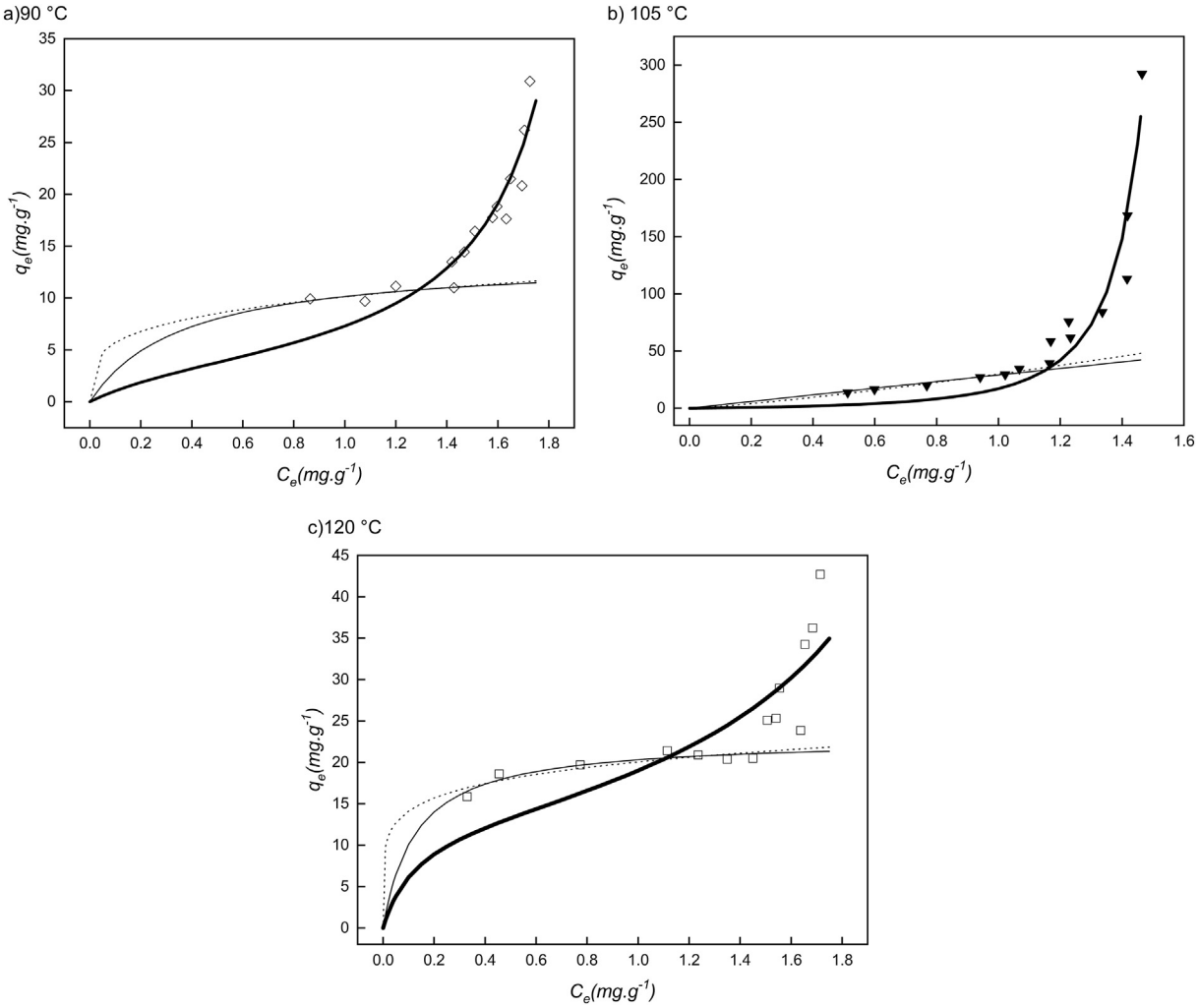

Fig. 7. Adsorption isotherm plots for carotenes onto NBE at (A) 90 °C, (B) 105 °C and (C) 120 °C. Representation: Experimental data – markers, modelled – lines: Langmuir (solid), Freundlich (dashed), BET (bold).

diameters, which restrain the oil flow inside the porous cavity and extra resistance to adsorption. The adsorption resistance is due to the diffusion across the liquid film surrounding the adsorbent particle. In fact, kinetics results showed that at this temperature, *equilibrium* was not achieved using NBE. At higher temperatures (105 and 120 °C), there were two steps, which can be attributed to the diffusion across the liquid film surrounding the adsorbent particle and the equilibrium step. The results were confirmed by the BET analysis, which shows that the pores of the acid adsorbent are larger than those of the neutral adsorbent.

3.3.3. Equilibrium

Equilibrium experiments were performed fixing the amount of crude oil and varying the amount of bleaching earth in a range from 0.1 to 9% (*w*/w). The curve fitting plot of experimental data are shown in Fig. 6 (ABE) and Fig. 7 (NBE). In both cases, it can be noted that carotenes adsorption occurs in two-steps: *(i)* for low bleaching earth/high carotenes content, the isotherms present unfavorable behavior, with the curve concavity facing upwards; *(ii)* for high bleaching earth/low carotenes concentration, the isotherms present favorable behavior. Moreover, the unfavorable region decreased with increasing the temperature. When comparing adsorption onto ABE and NBE, it can be seen that *equilibrium* concentration at the solid phase is higher for the acid adsorbent. The multi-step behavior of isotherms may be explained by a difference in pore sizes of bleaching earths or by different species of carotenoids being adsorbed. In fact, palm oil demonstrated the selective adsorption between α- and β-carotenes by Tonsil Opt 210 FF, being the last one preferably adsorbed (Ribeiro et al., 2018). Also, it indicated a strong competition for adsorption sites between adsorbed species or molecules from the solvent (Franco, Cunha, Dortzbacher, & Dotto, 2017).

Parameters for isotherms were determined by non-linear fitting: Langmuir and Freundlich parameters were determined only in the low adsorbent concentration region, as this models can not predict the unfavorable region. BET parameters were determined considering all studied concentration, in a two-step approach: firstly, the Langmuir parameter (K_S) was determined for low concentrations; this value was established and then the two other parameters were determined by non-linear fitting. Isotherm parameters and goodness of each model are summarized in Table 3.

Regarding the adsorption onto ABE, Langmuir model presented the higher correlation coefficients ($R^2_{adj} > 0.91$) followed by Freundlich ($R^2_{adj} > 0.87$) and BET ($R^2_{adj} > 0.82$). Lower coefficients for BET were expected, as parameters of this model were determined through more experimental data. For all other models and temperatures, statistical tests (*t*-test, f-test and *p*-value) showed a high accuracy between predicted and experimental data. Also, *t*-test revealed a high accuracy, i.e. t-values > than standard deviation. Similar results have already been reported in the literature. According to Silva et al. (2013), carotene adsorption onto Tonsil OPT 210 FF was better described by Langmuir.

Table 3
Isotherms constants for carotenes onto commercial bleaching earths at 90 °C, 105 °C and 120 °C.

		ABE					NBE				
Model	Parameters	90 °C	t-value	105 °C	t-value	120 °C	t-value	90 °C	t-value	105 °C	t-value	120 °C	t-value
Langmuir	K_s	22.91 ± 2.7	52.725	17.47 ± 2.24	38.5	12.38 ± 3.093	4.00						
	q_m	29.22 ± 0.5	8.365	40.67 ± 1.06	7.81	55.99 ± 3.83	14.63						
	R^2_{adj}	0.969		0.970		0.913							
	F-test	3063		1551		276							
	P-value (95%)	< 0.0001		< 0.0001		< 0.0001							
Freundlich	K_f	28.58 ± 0.7	43.43	39.92 ± 1.94	20.59	58.50 ± 4.010	14.58						
	n	0.145 ± 0.02	7.63	0.204 ± 0.04	5.262	0.311 ± 0.05	6.098						
	R^2_{adj}	0.941		0.870		0.903							
	F-test	1583		357		247							
	P-value (95%)	< 0.0001		< 0.0001		< 0.0001							
BET	K_s	22.91		17.47		12.38		2.74		8.56		7.88	
	K_l	0.44 ± 0.02	23.76	0.43 ± 0.03	14.60	0.58 ± 0.01	85.83	0.487 ± 0.015	33.26	0.659 ± 0.002	264.73	0.363 ± 0.051	7.137
	q_m	18.72 ± 1.7	11.26	27.24 ± 3.52	7.73	27.51 ± 1.84	14.93	4.43 ± 0.58	7.64	10.04 ± 1.47	6.83	13.06 ± 2.48	5.25
	R^2_{adj}	0.906		0.827		0.97		0.859		0.960		0.577	
	F-test	490		206		620		410		213		188	
	P-value (95%)	< 0.0001		< 0.0001		< 0.0001		< 0.0001		< 0.0001		< 0.0001	

*Ks(g/mg); qm (mg/g).

The adsorption rate (represented by the Langmuir parameter K_S) presented a negative correlation with temperature, i.e. increasing the temperature the affinity between adsorbent and adsorbate decreases. On the other hand, adsorptive capacity (represented by the Langmuir parameter q_{max} and by the Freundlich parameter K_F) increased with temperature, reaching the maximum at 120 °C, indicating an endothermic adsorption process (Pashai Gatabi, Milani Moghaddam, & Ghorbani, 2016). The Freundlich parameter n, which represents the surface heterogeneity has a positive correlation with temperature. The n ranges between 0 and 1 and it is a measure of adsorption intensity or adsorbent-adsorbate interaction heterogeneity (Pashai Gatabi et al., 2016). Interactions become more homogeneous as n value gets closer to zero (Foo & Hameed, 2010). Our results indicated that the effect of heterogeneity was more pronounceable at higher temperatures (Haghseresht & Lu, 1998).

Thus, modeling for the entire range of concentration was determined by BET model. Statistical tests (correlation coefficient, t-test, f-test and p-value) have shown that BET model was suitable to describe the adsorption process. The increase of equilibrium of adsorption for upper layers (K_l) and adsorption capacity of the monolayer (q_{max}) with temperature demonstrate the higher affinity between adsorbate and adsorbent at higher temperatures. Adsorptive capacity (q_{max}) estimated were lower than obtained by Langmuir, so studying adsorption in a narrow liquid concentration may overestimate monolayer capacity. The relation between equilibrium adsorption constant of mono and upper layers (K_s/K_l) ranged from approximately 20 to 50, demonstrating the high energy demanded multilayers formation.

Finally, the e*quilibrium* curves for carotenes adsorption onto NBE showed concavity facing upwards, what indicates a moderate attraction between adsorbent and adsorbate. Langmuir and Freundlich isotherms are not able to predict this behavior. Experimental data were fitted to BET model (Table 3). Statistical tests (t-test, f-test and p-value) showed a high accuracy between predicted and experimental data. The t-test revealed a high accuracy, i.e. t-values higher than standard deviation. BET model is suitable to predict carotenes adsorption onto NBE. Monolayer adsorption capacity (q_{max}) increased with temperatures, confirming that temperature increases adsorption capacity and process endothermicity. Considerably more adsorbent is required to remove the same amount of carotenes from palm oil when using NBE. K_s/K_l ranged from approximately 5 to 20, demonstrating lower energy differences between mono and upper layers formation in comparison with ABE. It was not found in literature previous work reporting carotenes adsorption neutral bleaching earths in similar concentrations.

3.3.4. Estimation of thermodynamic parameters

The isotherm experimental data were divided into two concentration regions: low bleaching earth (unfavorable) and high bleaching earth (favorable) and for each one the thermodynamic parameters were determined (Table 4). For all cases, the Gibbs Free Energy presented negative values, indicating that the adsorption process is feasible and spontaneous (Silva et al., 2014).

For ABE, at the favorable region, the magnitude of the Gibbs Free Energy increased with temperature, showing that adsorption is more spontaneous at higher temperatures. On the other hand, $\Delta H_{ads}{}^0$ was positive, indicating an endothermic process, i.e. an increase in temperature improves adsorption. This is also an indicator for a chemical adsorption process, as physisorption is always exothermic (Calligaris et al., 2018). Those results were in agreement with Sarier and Guler (1989), that stated that β-carotenes are chemisorbed onto acid activated bleaching earth. Ahmad, Chan, Abd Shukor, and Mashitah (2009) also found that β-carotene adsorption from hexane solutions onto silica gel was an endothermic process. There is an increase in entropy $\Delta S_{ads}{}^0$, which can occur due to a redistribution of the energy between that molecule and the adsorbent (Ahmad et al., 2009) or structural changes of the surface of the adsorbent, with the release of solvent molecules that gain translational entropy that compensates for the reduction of

Table 4
Equilibrium constants, standard Gibbs free energy, enthalpy and entropy of carotenes adsorption from Crude Palm Oil onto acid and neutral bleaching earths at 90 °C, 105 °C and 120 °C.

		ABE			NBE		
	T (°C)	*90*	*105*	*120*	*90*	*105*	*120*
Favorable	K_0	19.49	26.95	43.28	5.83	34.28	8.49
	ΔG	−8.97	−9.95	−11.38	−5.32	−10.67	−6.46
	ΔH	31.47			16.50		
	ΔS	0.11			0.06		
Unfavorable	K_0	21,622.72	3433.38	1304.79	31.07	23.48	1942.05
	ΔG	−30.14	−24.58	−21.66	−10.38	−9.53	−22.86
	ΔH	−111.50			161.09		
	ΔS	−0.23			0.47		

*ΔG (kJ/mol); ΔH (kJ/mol); ΔS (kJ/mol.K).

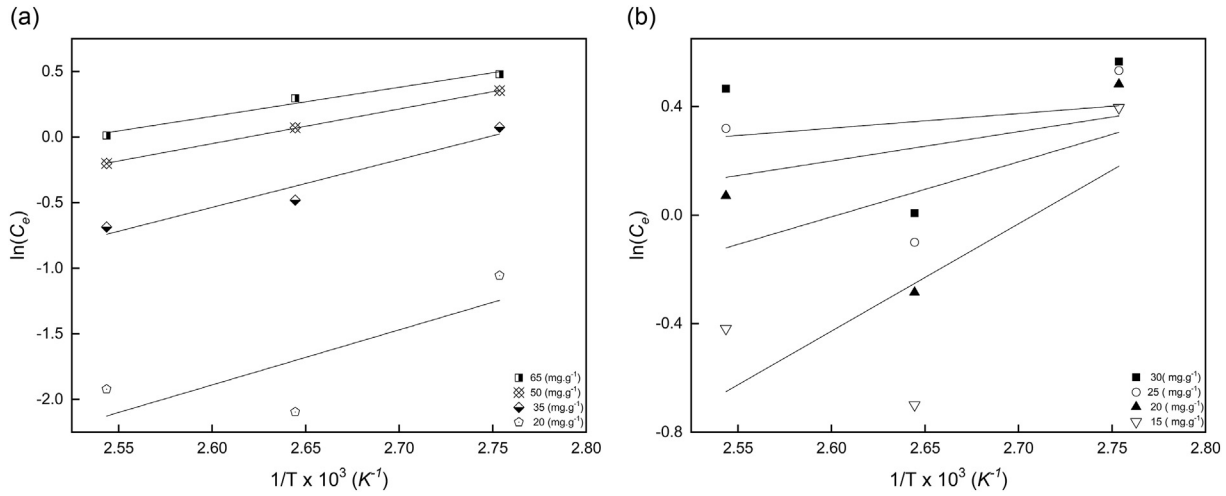

Fig. 8. Adsorption isosters used to determine the isoteric heat of carotenes onto ABE (a) and NBE (b).

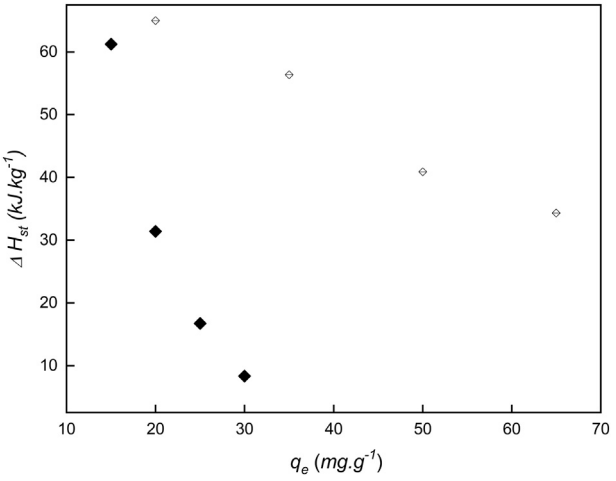

Fig. 9. $\Delta H_{st,\ a}$ as a function of the amount adsorbed of carotenes onto ABE (full symbol) and NBE (empty symbol).

entropy caused by adsorption of carotenes (Ajemba & Onukwuli, 2013). Similar results were found for carotenes adsorption onto acid activated bleaching earth (Silva et al., 2013), silica gel (Ahmad et al., 2009), sepiolite (Sabah, Çinar, & Çelik, 2007) and *nteje* clay (Ajemba & Onukwuli, 2013). At the unfavorable region of ABE, the enthalpy is negative, indicating an exothermic process. Entropy was also negative, indicating an increase of molecules organization and/or no structural changes in adsorbent surface. Negative entropy is reported when there is a thermodynamic compensation in adsorption process (Garvín et al., 2017). Indeed, a negative entropy may be attributed to an enthalpy-driven process and associative mechanisms. This same behavior was observed in previous studies of graphene oxides nanoparticles adsorption onto quartz (Sotirelis & Chrysikopoulos, 2015). These results suggested the formation of an activated complex between adsorbate and adsorbent during process occurring at high carotenes / low bleaching concentrations. In addition, it corroborates the increasing in adsorption energies heterogeneity, demonstrated by enthalpy change from positive to negative.

Regarding adsorption onto NBE, the magnitude of Gibbs Free Energy presented negative value for all temperatures. Enthalpy and entropy presented positive values for both favorable and unfavorable region, indicating an endothermic process and reorganization of complex adsorbate-adsorbent for all studied bleaching earth concentration range. Enthalpy results for the unfavorable region (higher than 40 kJ/mol) suggest monolayer formation, typical of chemical adsorption. On the other hand, the favorable region is related to multilayers adsorption (enthalpies lower than 40 kJ/mol) (Sabah et al., 2007).

3.3.5. Isosteric heat

Carotenes concentrations at a constant amount of adsorbed compounds were determined through BET isotherms. The isosteric heat of adsorption was obtained from the slope of the plot of ln (Ce) versus (1/T) for different amounts of adsorbed adsorbates (Fig. 8). The $\Delta H_{st,\ a}$ varied with surface loading for both adsorbents (Fig. 9), indicating that interaction heterogeneity between adsorbent and adsorbate. As a matter of fact, when there are energetic differences in the adsorbate/adsorbent interaction, due to different adsorption molecules or adsorption sites, the process will preferably occur at more energetic sites,

progressively going to the lower ones. Those results are in conformity with heterogeneity in adsorbent surface and multi-component adsorption. Systems presenting different interactions energy between adsorption sites and adsorbates (due to sites or adsorbates), adsorption will preferentially occur at higher energetic sites and it progressively goes to lower ones (Silva et al., 2013). A qualitative study performed with hybrid palm oil and the same adsorbents used in our study demonstrated β-carotene was preferably adsorbed than α-carotene, corroborating our results (Ribeiro et al., 2018). Slopes for all lines were similar for the process with ABE (Fig. 8a). Regarding NBE, slopes were more pronounced for adsorption at lower concentrations onto NBE (Fig. 8b), agreeing with thermodynamic results which suggest higher energies for monolayer formation. The same behavior was observed for adsorption onto ABE (Fig. 8a), although differences in slopes are much subtler. Positive values for $\Delta H_{st,\ a}$ (Fig. 9) confirmed adsorption was endothermic.

4. Conclusion

This work studied the adsorption process of hybrid palm oil carotenes onto two commercial adsorbents widely used in industry. Adsorbent characterization showed differences in pore volume and surface area and morphology. FTIR results evidenced water release after adsorption and changes on Si-O-Si bands, suggesting this is the most important adsorption site. Kinetic experimental data were well described by pseudo-first and pseudo-second-order models. Weber-Morris intra-particle diffusion model suggested the number of steps involved in the adsorption process depends on the adsorbent morphology and process temperature, since these parameters govern the oil capacity to enter inside pores. *Equilibrium* studies showed that the adsorption process was only favorable in low concentrations of carotene/high concentrations of adsorbent. Differences between the adsorption process with each bleaching adsorbent could be more easily observed at high concentration of carotenes / low concentration of adsorbent, when adsorption is unfavorable. For ABE, disfavor may be attributed to a complex adsorbent/adsorbate formation, evidenced by negative entropy. Whilst for NBE, it may be attributed to the high energy necessary to form a monolayer. For both adsorbents at the favorable adsorption region, enthalpy is positive (endothermic process), accompanied by positive entropy (molecules reorganization or release from adsorbent surface). Isosteric adsorption heat showed higher heterogeneity of the interaction between the adsorbate and the adsorbent for NBE than ABE, especially at lower adsorbent coverages.

Supplementary data to this article can be found online at https://doi.org/10.1016/j.foodres.2018.12.061.

Acknowledgments

The authors thank Embrapa Agroenergia for providing some facilities that were necessary for the development of this work. Simone Monteiro acknowledges CNPq (421852/2018-6), FAPDF (193.000.669/2015), FAPESP (2014/21252-0) and FINEP (01.13.0315.03) for the financial support. Erislene S. Almeida (381950/2015-8) acknowledges CNPq for the scholarship. The authors also acknowledge Oil-Dri, Clariant and Denpasa for kindly donating essential material for this work.

Declarations of interest

None.

References

Ahmad, A. L., Chan, C. Y., Abd Shukor, S. R., & Mashitah, M. D. (2009). Adsorption kinetics and thermodynamics of B-carotene on silica-based adsorbent. *Chemical Engineering Journal, 148*(2), 378–384. https://doi.org/10.1016/j.cej.2008.09.011.

Ajemba, R. O., & Onukwuli, O. D. (2013). Adsorptive removal of colour pigment from palm oil using acid activated nteje clay. Kinetics, equilibrium and thermodynamics. *Physiochemical Problems of Mineral Processing, 49*, 369. https://doi.org/10.5277/ppmp130133.

Alabarse, F. G., Conceição, R. V., Balzaretti, N. M., Schenato, F., & Xavier, A. M. (2011). In-situ FTIR analyses of bentonite under high-pressure. *Applied Clay Science, 51*(1), 202–208. https://doi.org/10.1016/j.clay.2010.11.017.

Alhamami, M., Doan, H., & Cheng, C.-H. (2014). A review on breathing behaviors of metal-organic-frameworks (Mofs) for gas adsorption. *Materials, 7*(4), https://doi.org/10.3390/ma7043198.

Alkan, M., Demirbaş, Ö., & Doğan, M. (2007). Adsorption kinetics and thermodynamics of an anionic dye onto sepiolite. *Microporous and Mesoporous Materials, 101*(3), 388–396. https://doi.org/10.1016/j.micromeso.2006.12.007.

AOCS (1998). *Methods and recommended practices of the American Oil Chemists' Society.* Champaign, IL: America Oil Chemists' Society.

Builes, S., Sandler, S. I., & Xiong, R. (2013). Isosteric heats of gas and liquid adsorption. *Langmuir, 29*(33), 10416–10422. https://doi.org/10.1021/la401035p.

Calligaris, S., Valoppi, F., Barba, L., Anese, M., & Nicoli, M. C. (2018). B-carotene degradation kinetics as affected by fat crystal network and solid/liquid ratio. *Food Research International, 105*, 599–604. https://doi.org/10.1016/j.foodres.2017.11.062.

Ceriani, R., Gonçalves, C. B., & Coutinho, J. A. P. (2011). Prediction of viscosities of fatty compounds and biodiesel by group contribution. *Energy & Fuels, 25*, 3712–3717. https://doi.org/10.1021/ef200669k.

Ebadi, A., Soltan Mohammadzadeh, J. S., & Khudiev, A. (2009). What is the correct form of bet isotherm for modeling liquid phase adsorption? *Adsorption, 15*(1), 65–73. https://doi.org/10.1007/s10450-009-9151-3.

España, M. D., Mendonça, S., Carmona, P. A. O., Guimarães, M. B., da Cunha, R. N. V., & Souza, M. T. (2018). Chemical characterization of the American Oil Palm from the Brazilian Amazon forest. *Crop Science, 58*(5), 1982–1990. https://doi.org/10.2135/cropsci2018.04.0231.

Foo, K. Y., & Hameed, B. H. (2010). Insights into the modeling of adsorption isotherm systems. *Chemical Engineering Journal, 156*(1), 2–10. https://doi.org/10.1016/j.cej.2009.09.013.

Franco, D. S. P., Cunha, J. M., Dortzbacher, G. F., & Dotto, G. L. (2017). Adsorption of Co (Ii) from aqueous solutions onto rice husk modified by ultrasound assisted and supercritical technologies. *Process Safety and Environmental Protection, 109*, 55–62. https://doi.org/10.1016/j.psep.2017.03.029.

Garvín, A., Ibarz, R., & Ibarz, A. (2017). Kinetic and thermodynamic compensation. A current and practical review for foods. *Food Research International, 96*, 132–153. https://doi.org/10.1016/j.foodres.2017.03.004.

Ghosal, P. S., & Gupta, A. K. (2017). Development of a generalized adsorption isotherm model at solid-liquid interface: A novel approach. *Journal of Molecular Liquids, 240*(Supplement C), 21–24. https://doi.org/10.1016/j.molliq.2017.05.042.

Gibon, V., De Greyt, W., & Kellens, M. (2007). Palm oil refining. *European Journal of Lipid Science and Technology, 109*, 315–335. https://doi.org/10.1002/ejlt.200600307.

Gonsalvesh, L., Marinov, S., Gryglewicz, G., Carleer, R., & Yperman, J. (2016). Preparation, characterization and application of polystyrene based activated carbons for Ni(Ii) removal from aqueous solution. *Fuel Processing Technology, 149*, 75–85. https://doi.org/10.1016/j.fuproc.2016.03.024.

Gurak, P. D., Mercadante, A. Z., González-Miret, M. L., Heredia, F. J., & Meléndez-Martínez, A. J. (2014). Changes in antioxidant capacity and colour associated with the formation of B-carotene epoxides and oxidative cleavage derivatives. *Food Chemistry, 147*, 160–169. https://doi.org/10.1016/j.foodchem.2013.09.106.

Haghseresht, F., & Lu, G. Q. (1998). Adsorption characteristics of phenolic compounds onto coal-reject-derived adsorbents. *Energy & Fuels, 12*(6), 1100–1107. https://doi.org/10.1021/ef9801165.

Ho, Y. S., & McKay, G. (1998). A comparison of chemisorption kinetic models applied to pollutant removal on various sorbents. *Process Safety and Environmental Protection, 76*(B4), 332–340.

Lampman, G. M., Kriz, G. S., Vyvyan, J. R., & Pavia, D. L. (2010). *Introduction to spectroscopy* (4th ed.). Bellingham, Washington: Western Washington University.

Liu, Y., Ying, D., Sanguansri, L., Cai, Y., & Le, X. (2018). Adsorption of catechin onto cellulose and its mechanism study: Kinetic models, characterization and molecular simulation. *Food Research International, 112*, 225–232. https://doi.org/10.1016/j.foodres.2018.06.044.

Maclellan, M. (1983). Palm oil. *Journal of the American Oil Chemists' Society, 60*(2Part2), 368–373. https://doi.org/10.1007/BF02543520.

Morishige, K., Tateishi, N., & Fukuma, S. (2003). Capillary condensation of nitrogen in Mcm-48 and Sba-16. *The Journal of Physical Chemistry B, 107*(22), 5177–5181. https://doi.org/10.1021/jp022137c.

Mozzon, M., Pacetti, D., Lucci, P., Balzano, M., & Frega, N. G. (2013). Crude palm oil from interspecific hybrid Elaeis oleifera × Elaeis guineensis: Fatty acid regiodistribution and molecular species of glycerides. *Food Chemistry, 141*(1), 245–252. https://doi.org/10.1016/j.foodchem.2013.03.0.

Ng, M. H., & Choo, Y. M. (2016). Improved method for the qualitative analyses of palm oil carotenes using Uplc. *Journal of Chromatographic Science, 54*(4), 633–638. https://doi.org/10.1093/chromsci/bmv241.

Norizzah, A. R., Nur Azimah, K., & Zaliha, O. (2018). Influence of enzymatic and chemical interesterification on crystallisation properties of refined, bleached and deodourised (Rbd) palm oil and Rbd palm kernel oil blends. *Food Research International, 106*, 982–991. https://doi.org/10.1016/j.foodres.2018.02.001.

Pashai Gatabi, M., Milani Moghaddam, H., & Ghorbani, M. (2016). Efficient removal of cadmium using magnetic multiwalled carbon nanotube nanoadsorbents: Equilibrium, kinetic, and thermodynamic study. *Journal of Nanoparticle Research, 18*(7), 189. https://doi.org/10.1007/s11051-016-3487-x.

Pirker, J., Mosnier, A., Kraxner, F., Havlík, P., & Obersteiner, M. (2016). What are the limits to oil palm expansion? *Global Environmental Change, 40*, 73–81. https://doi.org/10.1016/j.gloenvcha.2016.06.007.

Pohndorf, R. S., Cadaval, T. R. S., & Pinto, L. A. A. (2016). Kinetics and thermodynamics adsorption of carotenoids and chlorophylls in rice bran oil bleaching. *Journal of Food Engineering, 185*, 9–16. https://doi.org/10.1016/j.jfoodeng.2016.03.028.

Ribeiro, J. A. A., Almeida, E. S., Neto, B. A. D., Abdelnur, P. V., & Monteiro, S. (2018). Identification of carotenoid isomers in crude and bleached palm oils by mass spectrometry. *LWT - Food Science and Technology, 89*, 631–637. https://doi.org/10.1016/j.lwt.2017.11.039.

Sabah, E., Çinar, M., & Çelik, M. S. (2007). Decolorization of vegetable oils: Adsorption mechanism of B-carotene on acid-activated sepiolite. *Food Chemistry, 100*(4), 1661–1668. https://doi.org/10.1016/j.foodchem.2005.12.052.

Sampaio, K. A., Ayala, J. V., Silva, S. M., Ceriani, R., Verhé, R., & Meirelles, A. J. A. (2013). Thermal degradation kinetics of carotenoids in palm oil. *Journal of the American Oil Chemists' Society, 90*(2), 191–198. https://doi.org/10.1007/s11746-012-2156-1.

Sampaio, K. A., Ayala, J. V., Van Hoed, V., Monteiro, S., Ceriani, R., Verhé, R., & Meirelles, A. J. A. (2017). Impact of crude oil quality on the refining conditions and composition of nutraceuticals in refined palm oil. *Journal of Food Science, 82*(8), 1842–1850. https://doi.org/10.1111/1750-3841.13805.

Sarier, N., & Guler, C. (1989). The mechanism of B- carotene adsorption on activated montmorillonite. *Journal of the American Oil Chemists' Society, 66*(7), 917–923. https://doi.org/10.1007/BF02682609.

Silva, S. M., Sampaio, K. A., Ceriani, R., Verhé, R., Stevens, C., De Greyt, W., & Meirelles, A. J. A. (2013). Adsorption of carotenes and phosphorus from palm oil onto acid activated bleaching earth: Equilibrium, kinetics and thermodynamics. *Journal of Food Engineering, 118*(4), 341–349. https://doi.org/10.1016/j.jfoodeng.2013.04.026.

Silva, S. M., Sampaio, K. A., Ceriani, R., Verhé, R., Stevens, C., De Greyt, W., & Meirelles, A. J. A. (2014). Effect of type of bleaching earth on the final color of refined palm oil. *LWT – Food Science and Technology, 59*(2), 1258–1264. https://doi.org/10.1016/j.lwt.2014.05.028.

Sotirelis, N. P., & Chrysikopoulos, C. V. (2015). Interaction between graphene oxide nanoparticles and quartz sand. *Environmental Science & Technology, 49*(22), 13413–13421. https://doi.org/10.1021/acs.est.5b03496.

USDA. (2018). United States Department of Agriculture – Oilseed: World markets and trade. Retrieved January 31th, 2018.

Yousef, R. I., El-Eswed, B., & Al-Muhtaseb, A.a. H. (2011). Adsorption characteristics of natural zeolites as solid adsorbents for phenol removal from aqueous solutions: kinetics, mechanism, and thermodynamics studies. *Chemical Engineering Journal, 171*(3), 1143–1149. https://doi.org/10.1016/j.cej.2011.05.012.